



Model study on the stability of carbon support materials under polymer electrolyte fuel cell cathode operation conditions

L.C. Colmenares^{a,*}, A. Wurth^b, Z. Jusys^a, R.J. Behm^{a,*}

^a Institute of Surface Chemistry and Catalysis, Ulm University, D-89069 Ulm, Germany

^b TS-IM-IM-CB Inorganic Materials, Evonik Degussa GmbH, D-50997 Cologne, Germany

ARTICLE INFO

Article history:

Received 19 January 2009

Accepted 26 January 2009

Available online 6 February 2009

Keywords:

Carbon
Electrochemical oxidation
Corrosion
Start-up/shut-down
PEFC cathode
DEMS

ABSTRACT

The electrochemical oxidation and corrosion resistance of differently prepared and post-treated (graphitization, surface oxidation) carbon support materials, whose surface area and composition were characterized by adsorption measurements and X-ray photoelectron spectroscopy, were investigated in model studies performed under fuel cell cathode relevant potential conditions. These included also the abnormal cathode potentials (up to $1.5 V_{RHE}$) occurring during start-up and shut-down procedures. Reversible surface oxidation, leading, e.g., to the formation of quinones/hydroquinones, and irreversible oxidation to CO_2 were discriminated by combining electrochemical and on-line mass spectrometry measurements. Oxygenated surface carbon species were found to affect the surface area normalized electrooxidation activity much more than the surface area and porosity of the material, with graphitized carbon with low porosity and low oxygen surface content being most resistant towards reversible oxidation and towards irreversible oxidation at high potentials. Trapped CO_2 , formed upon carbon oxidation at high potentials, is proposed to be at least partly responsible for CO_2 release at low potentials, below the standard potential for electrochemical carbon oxidation.

© 2009 Elsevier B.V. All rights reserved.

1. Introduction

The efficiency and power density of polymer electrolyte fuel cells (PEFCs), which are considered as an alternative to combustion engines in electric vehicles and as small-scale stationary power supplies for portable electronics, are mainly limited by the kinetics of the oxygen reduction reaction (ORR) at the cathode side. In order to increase the catalyst utilization, Pt or Pt-alloy nanoparticles are dispersed on high surface area carbon supports. This way, high surface area carbon supported catalysts with high-performance and low metal loading have been developed [1–3]. The deterioration of the catalyst nanoparticles and of the carbon support, however, can strongly influence the long-term performance and durability of PEFCs, which is one of the crucial factors hindering the large-scale commercialization of this technology [2,4–6].

Among the various effects causing PEFC performance losses in fuel cell powered vehicles, catalyst degradation due to the electrochemical oxidation (corrosion) of the carbon support is one of the most important factors [4,7–10]. In earlier studies, two different reaction pathways for carbon oxidation have been distinguished, reversible oxidation to oxygenated surface carbon species such

as quinones/hydroquinones, lactones, carboxylates, etc. [11–17], and irreversible oxidation to CO_2 [7,8,10,18,19]. If the carbon is partly oxidized to oxygenated surface carbon species, the conductivity at the contact between the carbon support and the catalyst nanoparticles may decrease [20]. If the carbon is oxidized to CO_2 , catalyst nanoparticles may be lost from the support, resulting in a significant decrease of the catalyst active surface area, which in turn reduces the performance and operation lifetime of the PEFC [3,5–7,9,10,19,21–24]. The standard potential for the electrochemical oxidation of carbon to carbon dioxide is $0.207 V_{RHE}$ at $25^\circ C$ [25]. Therefore, under typical PEFC cathode operation conditions, carbon corrosion is not only thermodynamically feasible due to the high potentials (0.6–1.2 V) and high O_2 concentrations, but also kinetically enhanced by the elevated temperatures (50–90 °C) [9,12]. In addition, a decrease of the active surface area resulting from agglomeration of the catalyst particles or their losses due to carbon corrosion, can cause a significant variation of the oxygen reduction reaction pathways toward an increased hydrogen peroxide production even at cathode operation potentials [26–29], which can aggressively attack and oxidize carbon support and Nafion membrane, causing a rapid deterioration of the MEA.

The carbon corrosion rate can be increased also under abnormal PEFC operating conditions, referred to as “reverse-current decay mechanism”, which occur during fuel cell start-up and shut-down [30–33], when the anode compartment is partly filled with

* Corresponding authors.

E-mail addresses: luis.colmenares@uni-ulm.de (L.C. Colmenares), juergen.behm@uni-ulm.de (R.J. Behm).

hydrogen and air. This leads to the development of a hydrogen-air front over the active catalyst area, which can drive the cathode potential to extreme values where significant carbon-support corrosion can occur [31]. The cathode potential can exceed 1.5 V during start-up/shut-down [31], which in combination with the elevated PEFC operating temperature (50–90 °C), where the carbon oxidation kinetics are much faster than at ambient temperature [34], causes accelerated carbon corrosion and thus catalyst and electrode degradation. During a typical fuel cell automotive stack lifetime of about 5000 h, excursions to high potentials (e.g., 1.2 V_{RHE}) upon start-up/shut-down events are expected to occur approximately 30,000 times [35,36]. Therefore, in order to reduce the degradation of the fuel cell performance, alternative carbon materials with an improved corrosion resistance need to be developed.

The electrochemical carbon corrosion rate is not only a function of the temperature, electrochemical potential, and water partial pressure, but also the morphology of the carbon material plays an important role [12,13,37,38]. It has been proposed, that carbon materials containing more graphitic components exhibit a better corrosion resistance [12,13,35]. Furthermore, it is known that one can also reduce the corrosion rate of a carbon support by reducing the relative surface area of the support, e.g., by heat treatment (graphitization) [12,14,34,37]. Yu and Ziegler had shown that MEAs fabricated using catalysts supported on graphitized carbon are more resistant to carbon corrosion than comparable samples based on non-graphitized carbon supports, despite similar kinetic parameters (Tafel slope and activation energy) for the oxygen reduction reaction, and suggested that the morphology of the carbon mainly determines the carbon corrosion rate [35]. In addition to the structural effects, the corrosion behavior may also be affected by the coverage of oxygenated surface carbon groups such as quinones, lactones, carboxylic acids, etc. [12–17]. The surface of graphitized carbon is composed almost entirely of basal planes of carbon crystallites [37]. The basal planes of graphite are more resistant to electrochemical oxidation, which is more likely to occur at the edges of the basal planes [38]. Non-graphitized carbon materials, in which graphite crystallites are mixed with amorphous carbon, have a higher density of edges and unsaturated carbon bonds and hence can be attacked more easily by acidic electrolyte in model studies [12,37,39,40]. Most previous studies on carbon corrosion were performed in real fuel cells, where the measurements can be affected also by other problems, e.g., by insufficient catalyst utilization, problems with water management (drying of the membrane, flooding of the catalyst layer, etc.) or ill-defined mass transport. To avoid or reduce these problems, we investigated the corrosion of carbon support materials in model studies, where the reaction conditions are much better defined, and using close to fuel cell cathode operation potentials, even covering extreme (start-up/shut-down) conditions. In addition, these model studies allow a less time consuming and less costly preliminary evaluation of the electrochemical stability of carbon support materials; promising candidates can then be tested in real fuel cell measurements.

In the following, we will, after a brief description of the experimental procedures and set-up (Section 2) and of the physical characteristics of the different carbon materials (Section 3.1), describe the results of combined electrochemical and mass spectrometric measurements (potentiodynamic and constant potential) on reversible and irreversible surface oxidation, trying to elucidate correlations between the carbon structure and the surface oxygen content on the one hand and the electrochemical oxidation behavior on the other hand (Section 3.2). The carbon structure and surface oxygen content was varied by heat treatments and chemical (thermal) oxidation. Reversible oxidation to quinones/hydroquinones was distinguished from irreversible oxidation to CO₂ by on-line dif-

ferential electrochemical mass spectroscopy (DEMS), monitoring the $m/z=44$ signal. The electrochemical properties of the different carbon materials and their tendency towards reversible/irreversible oxidation as well as the influence of potential excursions to 1.5 V_{RHE} on these properties were characterized by cyclic voltammograms (CVs) recorded before and after a potential excursion to 1.5 V_{RHE} (Section 3.2.1). Next, carbon corrosion under start-up/shut-down conditions was evaluated by simultaneously monitoring the Faradaic current and the CO₂ formation rates during repetitive potential steps from 0.85 to 1.5 V_{RHE} and back (Section 3.2.2). Third, the effect of exposure to start-up/shut-down conditions on the carbon materials was tested in CVs recorded before and after a potential excursion to 1.5 V_{RHE} for 60 s, again following the Faradaic current and the CO₂ signal (Section 3.2.3). Finally, the ability of the selected samples to store CO₂ developed upon oxidation at higher potentials and to release this at lower potentials was investigated by Faradaic current and CO₂ signal transients recorded at 0.06 V_{RHE}, after exposure to CO₂ saturated solution at a potential where carbon oxidation to CO₂ is negligible (1.0 V_{RHE}) (Section 3.2.3).

2. Experimental

2.1. Materials

We investigated six different carbon materials, which were supplied by Evonik Degussa GmbH (Cologne, Germany). They can be divided into two groups: one set of three materials with low BET surface areas (set A) and another set with high BET surface area (set B). Each set included the non-treated raw material, graphitized material based on the respective raw materials, and graphitized-plus-oxidized ('graphitized/oxidized') material. The non-treated raw material were classified as A.0 and B.0; the graphitized material and the graphitized/oxidized material were denoted as A.1, B.1 and A.2, B.2, respectively (for physical characterization see Section 3.1). The supporting electrolyte (0.5 M sulfuric acid) was prepared using Millipore Milli-Q (18.2 MΩ cm⁻¹) water and ultrapure sulfuric acid (Merck, suprapur), and purged by high purity Ar (MIT Gase, N6.0) or saturated with CO₂ (MIT Gase, N5.0) in the electrolyte supply bottle. All measurements were performed at room temperature.

2.2. DEMS set-up

The DEMS set-up consists of a differentially pumped vacuum chamber equipped with a quadrupole mass spectrometer (Pfeiffer Vacuum, QM 422) and a computerized data acquisition system. It was described in detail elsewhere [41]. A dual thin-layer flow-through DEMS cell (for details see Refs. [42,43]) allows simultaneous measurements of the Faradaic current at a thin-film working electrode (see Section 2.4) and on-line detection of volatile species via a porous membrane (Scimat, 60 μm thick, 50% porosity and 0.2 μm pore diameter). The electrolyte flow was driven by the hydrostatic pressure in the supply bottle (electrolyte flow rate 60 μl s⁻¹).

Two Pt wires at the inlet and outlet of the thin-layer cell were used as the counter electrodes. The reference electrode (saturated calomel electrode, SCE) was connected to the outlet of the DEMS cell via a Teflon capillary. All potentials, however, are quoted against that of the reversible hydrogen electrode (RHE). The potential of the working electrode was controlled using a potentiostat from Pine Instruments.

2.3. Characterization of carbon materials

The surface area of the carbon materials was determined by adsorption measurements, using a TriStar BET surface area

and porosity analyzer (Micromeritics). X-ray photoelectron spectroscopy (XPS) measurements for determining the surface oxygen contents were performed on a PHI 5800 ESCA system (Physical Electronics), employing monochromatized Al K α radiation for excitation.

2.4. Preparation and characterization of electrodes

Thin-film working electrodes for the electrochemical measurements were prepared following the protocol described in Ref. [44]. Briefly, an aqueous suspension of the respective carbon material (2 mg ml⁻¹) was extensively ultrasonicated and then 20 μ l of the suspension were pipetted onto the middle part of mirror-polished glassy carbon disks (9 mm diameter, Sigradur GmbH, Germany). After evaporating the resulting water droplet in a N₂ stream, a similar pipetting/drying procedure was performed with an aqueous Nafion solution. The accessible geometric surface area of the resulting thin-film electrode was defined by a 50 μ m thick Kalrez O-ring, which served as gasket between electrode and cell body (diameter about 6 mm, geometric area 0.28 cm², carbon loading 142 μ g cm⁻²).

After installing the working electrode into the thin-layer flow cell, a stable base cyclic voltammogram was obtained by cycling the potential from 0.06 to 1.0 V_{RHE} in Ar-saturated supporting electrolyte (50 mV s⁻¹, 0.5 M H₂SO₄). For potentiodynamic measurements, the potential scan rate was reduced to 10 mV s⁻¹. During the potentiodynamic and potentiostatic measurements, the Faradaic and the mass spectrometer currents (CO₂ current, $m/z = 44$) were recorded simultaneously.

The CO₂ storage capacity of the high surface area carbon materials was determined by exposing the carbon electrode to CO₂-saturated 0.5 M H₂SO₄ solution for 60 s at 1.0 V_{RHE}, then the solution was exchanged to Ar-saturated supporting electrolyte, and finally the electrode potential was stepped from 1.0 to 0.06 V_{RHE} to induce CO₂ release.

3. Results and discussion

3.1. Physical characteristics

The surface area of the different carbon materials were determined by nitrogen adsorption (BET surface area), iodine and cetyl trimethyl ammonium bromide (CTAB) adsorption, where nitrogen and iodine adsorption measurements probe the total surface, including the inner surface of pores [12], while CTAB adsorption determines only the outer surface area, i.e., the inner surfaces of pores and voids are not included. Thus, the difference in surface areas obtained by nitrogen or iodine adsorption and by CTAB adsorption, respectively, reflects the inner surface area. These measurements led to the following results: carbon black A.0 is a coarse particle carbon black with a low BET and iodine adsorption surface area. The CTAB surface of this material is on the same level as the BET and iodine adsorption surface area. This means this material has a low porosity. The graphitization did not significantly change the surface areas of the carbon black A.1 compared to A.0, and the same is true for subsequent oxidation (material A.2). Carbon black B.0 is a very fine particle carbon black. The surface areas of this material are much higher compared to material A.0. The CTAB surface area of carbon black B.0 is substantially lower than the BET and iodine adsorption surface areas, reflecting a high porosity. Graphitization leads to a strong decrease of the surface areas. Iodine and BET surfaces are decreased by about 75%, and the CTAB surface decreases by about 50% relative to B.0. The decrease in the total surface area upon heat treatment, as determined by nitrogen or iodine adsorption, can be caused by thermally induced closing or removing of the pores [12]. The CTAB surface area of carbon black B.1 is on the

same level as the BET and iodine adsorption surface area, i.e., the porosity of the graphitized carbon black B.1 is very low. Similar to A-type carbon black, subsequent oxidation does not change the surface areas of the graphitized carbon black B.1, reflecting similar structural properties in B.1 and B.2.

The surface areas were determined ex situ, prior to the thin-film preparation and electrochemical measurements, and therefore the properties in the thin-film electrodes during the electrochemical measurements in acidic electrolyte (0.5 M H₂SO₄) may be somewhat different. Nevertheless, the ex situ determined characteristics are useful to correlate the influence of the structural and surface chemical properties (oxygen-containing surface groups) with the corrosion behavior of these carbon materials.

It is known that the heat treatment of carbon involves a displacement and rearrangement of the layer planes and small crystallites to achieve crystalline layers on the surface [12], which is referred to as graphitization process (conversion of amorphous carbon to graphite). The results summarized above suggest that for both types of carbon materials heat treatment leads to more or less pronounced structural changes, as can be concluded from the overall surface area (including pores) measured by nitrogen and iodine adsorption and the outer surface area detected by surface-sensitive CTAB measurements. Depending on the porosity, reactive species (or nitrogen, iodine in the adsorption measurements) can enter the inner regions of the carbon particles. The graphitic character of the outer and possibly also of the inner surface can influence the electrochemical reactivity and the corrosion resistance of the corresponding carbon materials as well, either by encapsulation (graphitization of the outer layers) of an amorphous and corrosion sensitive core, or by graphitization of inner and outer surfaces (see below).

Carbon samples with a highly graphitic character due to surface graphitization, e.g., A.1 and B.1, contain a high fraction of basal-plane oriented graphite surface, whereas samples with a high content of amorphous carbon exhibit a much higher fraction of defects, edges and unsaturated carbon bonds (e.g., sample B.0) [37]. From ethene adsorption isotherms on carbon blacks, Schröder et al. derived that adsorption sites on the basal-plane (sp² hybridization) represent low energy adsorption sites compared to the higher adsorption energies at sp³ hybridized sites [45]. Similar effects are expected for oxygen adsorption. Because of the correlated higher barrier for oxygen dissociation on the basal plane compared to that at edge sites [46], the sensitivity of the basal-plane graphite surface towards surface oxidation is much lower than that of amorphous carbon with many edge sites [12,37,38]. This trend is illustrated by the surface oxygen content of the different carbon materials (Table 1). Comparing the raw materials A.0 and B.0 with each other, the surface oxygen content increase with increasing surface area to almost the double value in B.0 compared to A.0. Comparing the raw materials (A.0 and B.0) with the corresponding graphitized samples (A.1 and B.1), the oxygen content decreases considerably, to about 35–40% of the initial value, upon increasing the degree of crystalline surface order (graphitic character) by heat treatment (surface graphitization). Subsequent oxidation of the graphitized samples leads to the following results: the BET surface area of the graphitized/oxidized samples (A.2 and B.2) increases only little compared to the respective graphitized samples (A.1 and B.1). This may be explained by slow pore formation via complete oxidation to CO₂, while simultaneous surface oxidation to oxygenated surface carbon species does not affect the specific surface area. On the other hand, the surface oxygen content increases to more than double of the initial value in the A.0 and B.0 materials, respectively, reflecting considerable reaction with oxygen. Considering the little change in surface area, the reaction leads mainly to partially oxidized surface carbon species (quinones, lactones, etc.).

Table 1

Surface oxygen content, and surface area (BET) normalized CO₂ charge (DEMS) generated during a potential excursion from 0.85 to 1.5 V_{RHE} during 60 s (transients #1–#3) on the same carbon electrode on different carbon materials.

Carbon samples	Oxygen/atomic%	CO ₂ generation/nC m ⁻²		
		Transient #1	Transient #2	Transient #3
(A.0) Non-treated carbon	0.44	867.6	804.8	712.4
(A.1) Graphitized carbon	0.17	343.9	229.1	196.5
(A.2) Graphitized/oxidized carbon	1.15	2125.1	1181.3	910.0
(B.0) Non-treated carbon	0.80	746.5	739.7	683.5
(B.1) Graphitized carbon	0.28	323.9	245.4	228.3
(B.2) Graphitized/oxidized carbon	1.68	1712.4	1005.0	801.0

3.2. Electrochemical characteristics

The electrochemical oxidation of the six carbon materials was evaluated by simultaneous electrochemical and on-line mass spectrometry (CO₂⁺ ion current, $m/z = 44$) measurements. This way, we can discriminate between reversible carbon surface oxidation (formation of quinone/hydroquinone redox couples), which is detected by the Faradaic current only, or irreversible oxidation to CO₂, which shows up both in the Faradaic current and in the $m/z = 44$ mass spectrometric current.

3.2.1. Cyclic voltammetry characteristics

Figs. 1 (set A) and 2 (set B) show the stable CVs (upper plots: a, c and e) of the corresponding carbon materials before (CV-1) and after (CV-2) a series of three potential excursions to 1.5 V_{RHE}. The experimental protocol of the potential excursions is given in Section 3.2.2 CV-2 was recorded after stepping back to 0.85 V_{RHE}, and cycling several times between 0.06 and 1.0 V_{RHE} until a stable CV was obtained. Simultaneously, the CO₂ formation was recorded in mass spectrometric cyclic voltammograms (MSCVs, lower plots: b, d and f).

First of all, we find significant differences in the double layer capacities of the different materials, which is most clearly evident

in the currents at ca. 0.2 V. The double layer capacities scale with the total surface areas of the different samples, with higher values for the B-type samples than for the A-type sample, and in particular for the B.0 sample. After excursion to high potential, the Faradaic currents (CV-2) show for all carbon materials studied an increase in the double-layer current, which is most significant for the samples A.0, B.0 and B.1, and the appearance of a pair of anodic and cathodic peaks, respectively, at about 0.5–0.6 V_{RHE}. The latter peaks can be assigned to the formation of quinones and their reduction to hydroquinone, i.e., to the reversible oxidation and reduction of oxygenated surface carbon species [11,12]. This redox feature is more pronounced on the raw carbon materials than on the processed (graphitization and graphitization/oxidation) carbons. Thus, the increase in the reversible carbon oxidation/reduction current depends on the state of the initial carbon surface, including both structure and chemical composition, before the high-potential treatment. As discussed above (Section 3.1), the non-treated materials, in particular the B-type materials, exhibit a higher inner surface area (porosity) compared to heat treated samples, which may be accessible to the electrolyte and lead to an increase in the reversible carbon oxidation. The increase of the total carbon surface area is reflected also by an increase of the double-layer capacity. Similar observations were reported also by Paik et al.

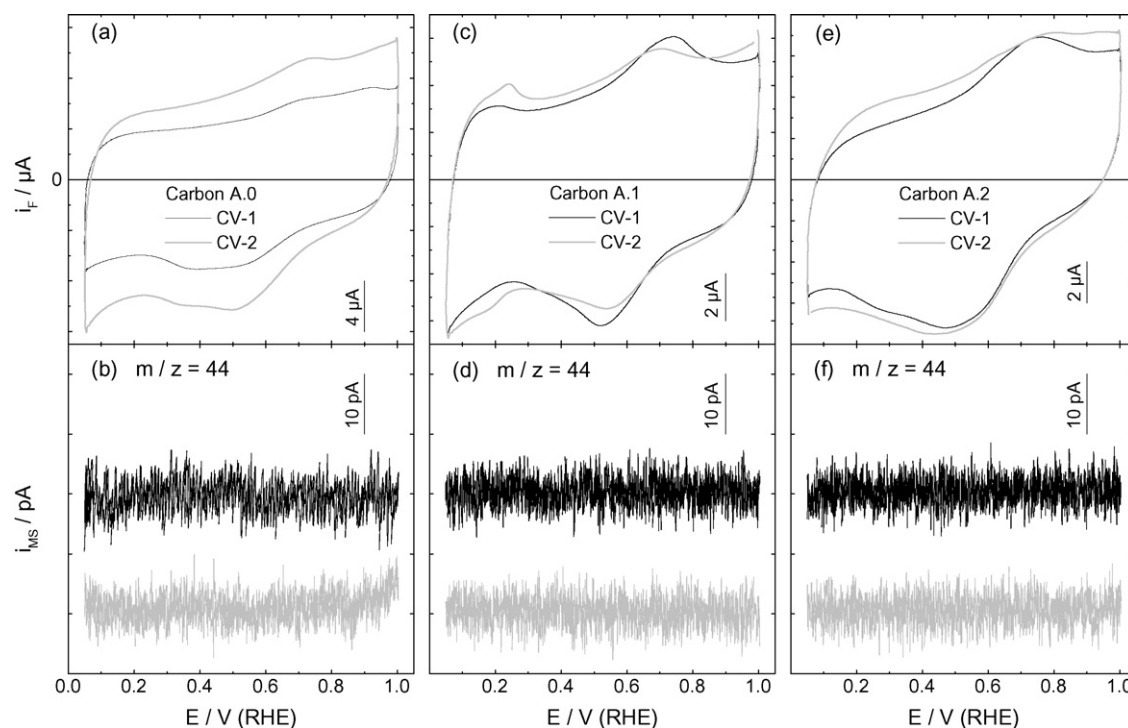


Fig. 1. Simultaneously recorded stable Faradaic current (a, c and e) and mass spectrometric cyclic voltammograms (b, d and f) of non-treated (A.0), graphitized (A.1) and graphitized/oxidized (A.2) carbon materials before (CV-1) and after (CV-2) a set of three potential excursions to 1.5 V_{RHE} (time at 1.5 V_{RHE} 60 s each) in Ar-saturated 0.5 M H₂SO₄ at room temperature (scan rate 10 mV s⁻¹, electrolyte flow rate ca. 60 μl s⁻¹, experimental protocol see text).

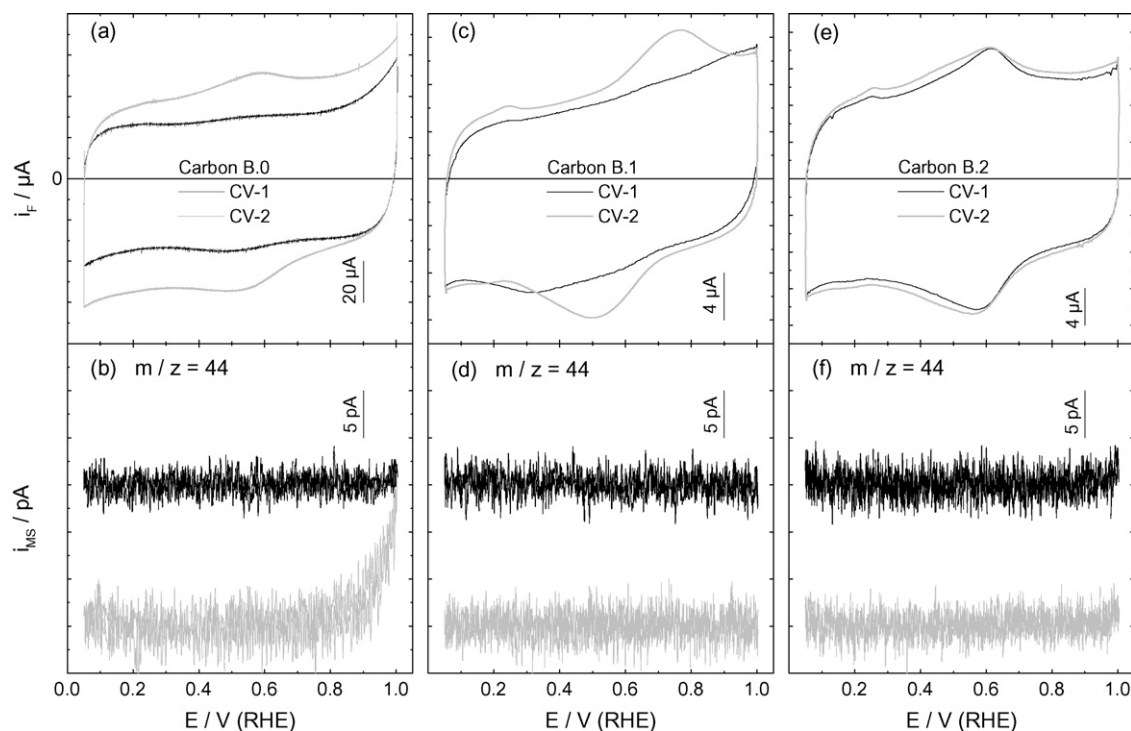


Fig. 2. Simultaneously recorded stable Faradaic current (a, c and e) and mass spectrometric cyclic voltammograms (b, d and f) of non-treated (B.0), graphitized (B.1) and graphitized/oxidized (B.2) carbon materials before (CV-1) and after (CV-2) a series of three potential excursions to $1.5 V_{\text{RHE}}$ (time at $1.5 V_{\text{RHE}}$ 60 s each) in Ar-saturated $0.5 M H_2SO_4$ at room temperature (scan rate $10 mV s^{-1}$, electrolyte flow rate *ca.* $60 \mu l s^{-1}$, experimental protocol see text).

[47], who equally found an increase in double-layer charge, which depended on the accumulated exposure time at high potentials, where the electrochemical oxidation of carbon increases the density of carbon surface defects. This oxidative treatment also leads to a higher surface coverage of oxygenated surface species and thus increases the wettability of the carbon surface [12,15,48]. After electrochemical oxidation of the graphitized sample B.1, the shape of the CV-2 approaches that of the CVs obtained for the graphitized/oxidized B.2 carbon sample (high oxygen content). On the graphitized/oxidized sample B.2, in contrast, the electrochemical oxidation has a much lower effect. Also on the samples A.1 and A.2 with their much lower surface area the effect of electrooxidation is much less pronounced.

Most astonishing is the observation that prior to the high-potential treatment the graphitized sample B.1 is essentially inert against reversible oxidation/reduction, while after electrochemical corrosion it shows reversible oxidation–reduction peaks similar to those observed on the other samples. The origin for this behavior is not yet resolved, but it is not related to differences in the surface area or the oxygen content of the initial samples.

Stonehart suggested that the removal of oxygenated surface species leads to the formation of micropores, thereby increasing the surface area of the carbon and the probability for further corrosion [49]. A different mechanism for enhancing the surface area was put forward by Thiele [39]. He concluded that sulfuric, nitric, hydrochloric, perchloric and hydrofluoric acids penetrate into the interior of the graphite, resulting in graphite swelling and in a lamellar structure. (Note that graphite swelling is not completely reversible.) This way, the carbon atoms in the internal lattice planes become accessible to oxidation. The slight differences in the peaks of the redox couples (reversible oxidation/reduction to quinones/hydroquinones and other carbonyls) observed in the CVs on the different carbon materials could indicate differences in the mix of the surface functional groups produced after excursion to high potentials [50].

The corresponding CO_2 signals before (CV-1) and after (CV-2) exposure of the carbon electrodes to high potential are shown in Figs. 1 and 2 (lower plots: b, d and f, respectively). The majority of the carbon materials studied, except of sample B.0, did not show significant changes in the amount of generated CO_2 after electrochemical pre-oxidation of the carbon samples at high potentials. In contrast, the sample B.0 (non-treated material) showed an earlier onset of the CO_2 signal at potentials above $0.8 V_{\text{RHE}}$ compared to the other samples. Hence, the porous structure of the high surface area material B.0 can be modified by the high potential electrooxidation such that it is more reactive towards oxidation to CO_2 even at potentials where before the electrooxidation treatment this was not observed. This may be related to the larger number of reactive defects after high potential electrooxidation, including structural defects as well as chemical modifications (oxygenated surface species).

3.2.2. Carbon corrosion rates

Under automotive fuel cell operation conditions, the PEFC cathode undergoes short excursions to high potentials during the start-up procedures ($E > 1.2 V_{\text{RHE}}$) [35,36]. Therefore, the specific carbon corrosion rates (i.e., the current density for CO_2 formation, normalized to the BET surface area) of the six different carbon materials were compared among each other in potential step measurements to high potential ($1.5 V_{\text{RHE}}$) and back. Faradaic (Fig. 3a and c) and mass spectrometric ($m/z=44$) current transients (Fig. 3b and d) upon the potential step from $0.85 V_{\text{RHE}}$ (the potential was held for 120 s at this potential, after recording a CV) to $1.5 V_{\text{RHE}}$, holding there for 60 s and then stepping back to $0.85 V_{\text{RHE}}$, are shown in Fig. 3. This procedure was repeated 3 times (transients #1–#3) on the same electrode and the CO_2 charge density (normalized vs. the corresponding BET carbon surface area of the initial material) was determined in each case (see Table 1). The holding time at $0.85 V_{\text{RHE}}$ was 120 s each time.

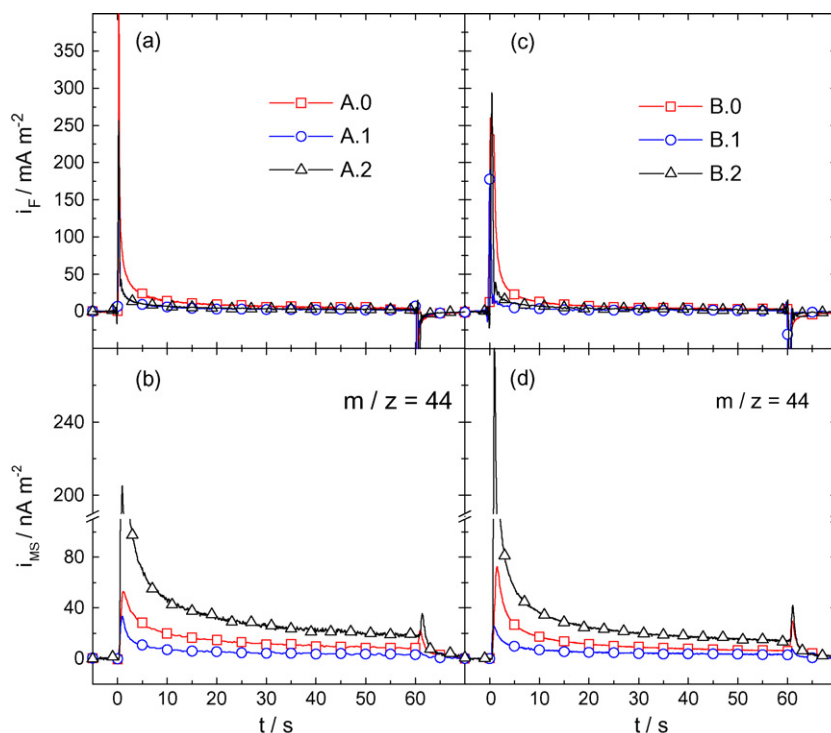


Fig. 3. Chronoamperometric transients of the Faradaic (a and c) and the mass spectrometric (b and d) currents recorded simultaneously after a potential step from 0.85 to 1.5 V_{RHE} and back to 0.85 V_{RHE} , reflecting carbon oxidation to CO_2 on non-treated (A.0 and B.0), graphitized (A.1 and B.1) and graphitized/oxidized (A.2 and B.2) carbon in Ar-saturated 0.5 M H_2SO_4 at room temperature (electrolyte flow rate ca. $60 \mu l s^{-1}$). The current density is normalized to the BET surface area of the respective carbon material.

Upon stepping the potential to 1.5 V_{RHE} , the Faradaic current transients (Fig. 3a and c) exhibit an initial spike, which may result from pseudo-capacitive charging, irreversible oxidation of pure carbon and/or oxygenated surface carbon species to CO_2 and/or reversible formation of the latter species. Subsequently, the Faradaic current decays continuously until reaching an approximately constant steady-state value. Returning the potential from 1.5 to 0.85 V_{RHE} , the electrochemical current also shows a marked cathodic current spike, which may be related both to capacitive contributions and to the reduction of surface oxy-species.

Also the mass spectrometric CO_2 signals ($m/z = 44$, Fig. 3b and d), which reflect the oxidative formation of CO_2 without interference with other contributions present in the Faradaic current response such as double-layer charging or surface oxidation, resolve clear spikes when stepping to 1.5 V_{RHE} . These spikes, however, are much less pronounced than the Faradaic current spikes. The difference between the Faradaic current spike and the CO_2 current spike is at least largely attributed to the dominant capacitive contributions in the Faradaic current and to the smear out of the CO_2 signal due to the limited time resolution of the thin-layer flow cell (ca. 1 s). The spike in the CO_2 signal clearly demonstrates a fast initial CO_2 formation, which may result either from direct oxidation of carbon or from further oxidation of pre-formed surface oxy-species to CO_2 . With time, the CO_2 formation rates approach a steady-state value, which corresponds to the continuous oxidation of carbon and/or oxygenated carbon surface species to CO_2 under these conditions. The BET surface area normalized CO_2 formation rates determined from these steady-state data show a clear effect of the carbon pre-treatment procedure: the rates under steady-state conditions are highest for the graphitized/oxidized samples, lower for non-treated materials, and even slightly lower for the graphitized samples, in agreement with recently reported findings of an improved corrosion stability of graphitized carbon support compared to non-graphitized carbon [19]. The situation is similar when comparing the BET surface area normalized total amounts of CO_2 formed upon 60 s carbon oxida-

tion at 1.5 V_{RHE} (Table 1) of the corresponding carbon samples. In this case, however, the differences are much more pronounced, with the amount of CO_2 formed on the graphitized/oxidized materials (A.2 and B.2) being about 4–6 times higher than on the graphitized samples (A.1 and B.1). The decreasing tendency for CO_2 formation correlates well with the amount of surface oxygen on these samples (see Table 1), while the BET surface areas in each group (A.1 and A.2; B.1 and B.2) are of comparable magnitude. Hence, the presence of oxygenated surface carbon species increases the tendency for CO_2 formation during a potential excursion to highly anodic potentials (here 1.5 V_{RHE}). This result agrees well with a proposal by Giordano et al., who postulated that the oxygen groups present on the surface of carbon black enhance the corrosion rate [14]. The small spike present for all catalysts after stepping back the potential to 0.85 V_{RHE} is attributed to the release of ‘trapped’ CO_2 , which was generated at high potential, from the carbon structure (see Section 3.2.3).

Returning to the Faradaic currents in Fig. 3a and c, the apparent initial electrochemical oxidation rate, given by the maximum current density (normalized to the BET surface area), is much higher on the non-treated carbon sample A.0 than on the post-treated carbon materials A.1 and A.2, while for the B-type materials these differences are less pronounced. With time, the oxidation currents decay rapidly towards a steady-state value. Considering that (i) the initial spike in the CO_2 formation signal and the maximum rate for surface area normalized CO_2 formation are much lower on the A.0 sample than on the A.2 sample, and that (ii) the pseudo-capacitive effects should scale roughly with the BET surface area, the very high Faradaic current density spike obtained for the A.0 sample points to a rapid reaction to oxygenated surface species on that sample, e.g., due to specific effects caused by small scale roughness and a highly defective carbon surface. In contrast, the post-treated samples are more resistant to the build-up of oxygenated surface species (see the rather similar redox peaks in the corresponding CV-1/CV-2 pairs in Figs. 1 and 2). The somewhat higher peak for the initial Faradaic

current density of sample B.1 compared to B.0 is explained by a higher tendency to form oxygenated surface species, in the same way as discussed in the previous section (Fig. 2c).

The charge densities related to carbon dioxide formation during exposure of the carbon electrodes to $1.5 V_{\text{RHE}}$ during 60 s are summarized in Table 1 (transients #1–#3). With increasing number of high-potential excursions, the amount of CO_2 formed decreases, a similar behavior was observed for all samples. This decrease in CO_2 formation can be explained by a decrease in active carbon sites, either structurally dominated active sites such as defects or chemically dominated active sites such as oxygenated surface carbon species for CO_2 formation with ongoing oxidation. A similar decay of the carbon corrosion current with time was also reported by Giordano et al. for carbon black in H_3PO_4 [14] and by Li et al. for carbon nanotubes in H_2SO_4 [51,52].

The data in Table 1 demonstrate that for both sets of carbon materials studied (sets A and B), the graphitization (samples A.1 and B.1) leads to a decrease of corrosive CO_2 formation compared to that for the non-treated materials (cf. samples A.1 \rightarrow A.0, B.1 \rightarrow B.0). Comparing this with the changes in surface area upon heat treatment, which are pronounced for the B-type materials (B.0 \rightarrow B.1), but essentially absent in A-type materials (A.0 \rightarrow A.1), the surface area has little effect on the surface area normalized amount of corrosive CO_2 formation. (The surface area normalized CO_2 formation charge is used to discriminate between effects purely related to a higher surface area and effects related to a change in the inherent activity of the surface.) A better correlation is found between surface area normalized CO_2 formation and the surface oxygen content. For both sets of samples, the oxygen content decreases after the heat treatment, and increases sharply upon subsequent thermal oxidation, which parallels the trends in surface area normalized CO_2 formation (Table 1). Hence, the oxygen content plays an important role for the electrochemical carbon corrosion activity, and the oxygen-containing species on the carbon surface can be considered as active centers for further electrochemical oxidation to CO_2 . The oxidation treatment is also known as “burn-off” or “activation” process, leading to oxidized carbon (“activated carbon”) [12]. If graphitized (A.1 and B.1) and graphitized/oxidized (A.2 and B.2) samples of the respective sets are compared with each other, the effect of the oxygen content (related to the activated carbon area) on the corrosion rates is again recognized. In both cases (A.2 vs. A.1 and B.2 vs. B.1), the BET carbon surface areas are quite similar, but the oxygen content increases significantly after activation (oxidation) of the graphitized sample. The latter agrees well with the distinct increase in CO_2 formation for the graphitized/oxidized samples (see Table 1). It should be noted, however, that strictly speaking this correlation between corrosion activity and surface oxygen content is possible only for the first potential step to $1.5 V_{\text{RHE}}$, while in the subsequent potential excursions the content of surface oxy-species is not known, due to the undefined amount of oxygenated surface carbon species formed in the preceding potential excursion(s).

3.2.3. CO_2 generation at low potentials

After the electrochemical oxidation of the carbon samples at high potentials ($1.5 V_{\text{RHE}}$) in potential step experiments (see Fig. 3), we detected an increased CO_2 generation when stepping back to lower potential ($0.85 V_{\text{RHE}}$). The intensity of this peak depends on the carbon material. Recently, several groups observed the generation of CO_2 at low potentials even below the standard potential for carbon ($E = 0.207 V_{\text{RHE}}$ [25]) during potentiodynamic, potentiostatic and start-up/shut-down experiments on pure carbon and on carbon supported Pt catalysts [18,33,53,54]. They proposed that the CO_2 generated at low potentials can result (i) from chemical carbon oxidation by hydrogen peroxide [18,53,53], which is produced by oxygen reduction on hydroquinone modified carbon [12,55,56] or

by direct oxygen reduction on Pt at low potentials [27,28,57,58], and (ii) by release of adsorbed or trapped CO_2 upon reduction of the oxygenated surface carbon species [18].

The possibility of CO_2 storage in the carbon material, during oxidative CO_2 formation at high potentials and its subsequent potential induced release was explored in a set of potentiodynamic and transient experiments. In the first set, following the above potential step experiments (Fig. 3 and Table 1), the potential was held at $0.85 V_{\text{RHE}}$ for 120 s after the last potential excursion (transient #3), then scanned from 0.85 to $0.06 V_{\text{RHE}}$ and back (2 cycles) and finally between 0.06 and $1.0 V_{\text{RHE}}$ in order to compare with the initial CVs. During the potentiodynamic measurements, the CO_2 generation was simultaneously followed by on-line mass spectrometry. The results of these experiments are shown in Figs. 4 and 5 for the samples from sets A and B, respectively. The upper plots (a, c and e) correspond to the Faradaic current, the lower plots (b, d and f) to the mass spectrometric $m/z = 44$ ion current.

Figs. 4a, c and e and 5a, c and e, respectively, show the first cyclic voltammogram immediately after the potential step experiments (CV-1) and the stable cycle after three following cycles (CV-2). In the first negative-going scan in CV-1, we observed an increasing reduction current for all carbon materials for potentials $< 0.8 V_{\text{RHE}}$, and then, after passing through a maximum, a more or less pronounced current decrease of the reduction current. The reduction current is attributed to the electrochemical reduction of part of the oxygen-containing species formed on the carbon surface while keeping it at high potential [18]. The exact shape of the current response in the negative-going scan depends on the carbon material. The reduction current is most pronounced for the non-treated carbon samples A.0 and B.0 (Figs. 4a and 5a, respectively) and less pronounced for the graphitized samples A.1 and B.1 (Figs. 4c and 5c) and the graphitized/oxidized samples A.2 and B.2 (Figs. 4e and 5e). In the subsequent cycles, the reduction current decreases and approaches a reproducible CV when not exceeding the positive potential limit of $1.0 V_{\text{RHE}}$ (grey lines in Figs. 4a, c and e and 5a, c and e).

The lower plots in Figs. 4 and 5 show the CO_2 generation during the respective potential cycles. In general, the CO_2 generation is more pronounced on the B-type samples than on A-type samples, which almost quantitatively scales with the BET surface area. For the graphitized samples CO_2 formation is very low (B.1) or essentially absent (A.1). Considering the standard potential for the oxidation of carbon to CO_2 of about $0.207 V_{\text{RHE}}$ at 25°C [25], CO_2 can obviously be formed or released at potentials below the reversible potential of electrochemical carbon oxidation. Similar observations have also been reported by other groups [33], and were explained by chemical reaction [18,53,54] of hydrogen peroxide, which was produced on the carbon surface, with carbon at these cathodic potentials [18,53].

Alternatively, the observation of CO_2 at low potentials could be explained by release of CO_2 which was generated during carbon electrooxidation at high potentials and then adsorbed on the carbon surface or trapped and stored in carbon pores. CO_2 could be ‘stored’ by stable adsorption on the carbon surface, e.g., on structural defects on the carbon surface (‘active sites’) or by interaction with oxygenated surface species present on the (inner) carbon surface, or stabilized in nanopores of the carbon material. Recently, Liu et al. [59] published electron microscopy images of oxidized carbon particles containing central voids (center-hollowed particles). These voids were either isolated or interconnected and either closed or open with exit channels to the surfaces of the carbon. These authors also concluded that the corrosion of carbon nanoparticles proceeds from the center toward the surface. Stable chemisorption of CO_2 on active carbon sites forming surface carbon–oxygen complexes was calculated by Montoya et al. [60]; in the presence of oxygen-containing groups, formation of surface carbonates was proposed [60,61]. At higher coverages, CO_2 was found to inter-

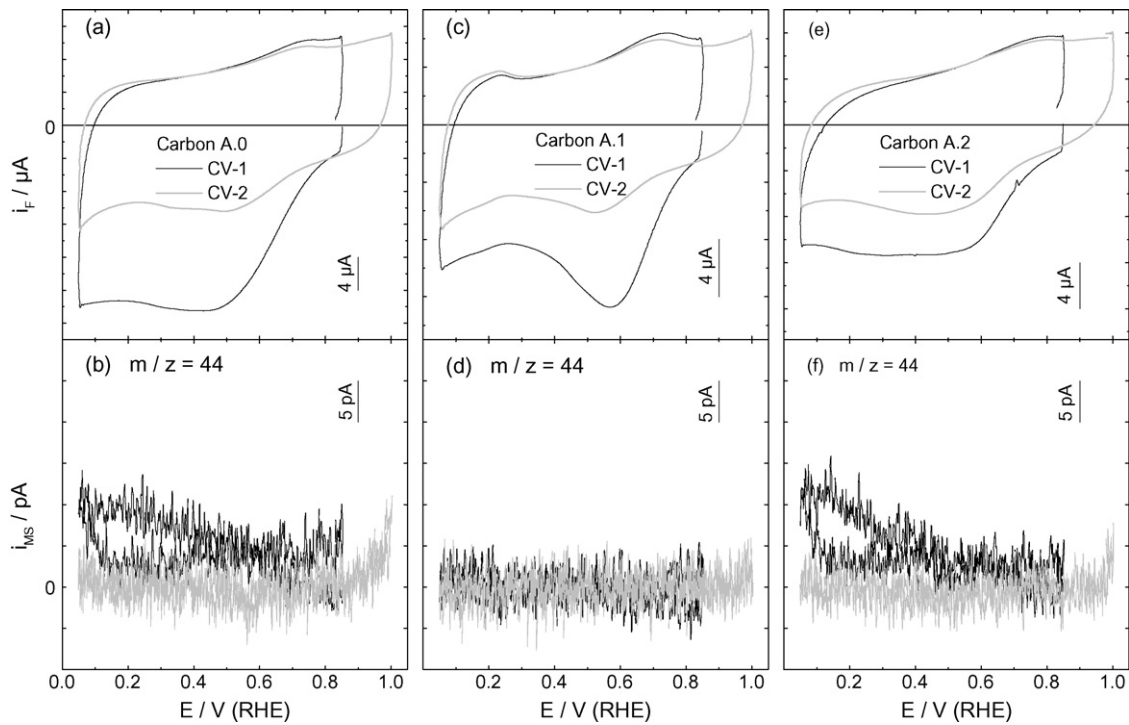


Fig. 4. Potential-dependent CO_2 generation: simultaneously recorded Faradaic (a, c and e) and mass spectrometric currents (b, d and f) on non-treated (A.0), graphitized (A.1) and graphitized/oxidized (A.2) carbon materials after a sequence of three potential excursions to $1.5V_{\text{RHE}}$ (holding time 60 s) and subsequent return to $0.85V_{\text{RHE}}$ (holding time 120 s) in Ar-saturated $0.5\text{ M H}_2\text{SO}_4$ at room temperature. CV-1 represents the initial CV after the potential excursion and CV-2 represents the stable CV after cycling the potential several times between 0.06 and $1.0V_{\text{RHE}}$ (scan rate 10 mV s^{-1} , electrolyte flow rate ca. $60\ \mu\text{l s}^{-1}$).

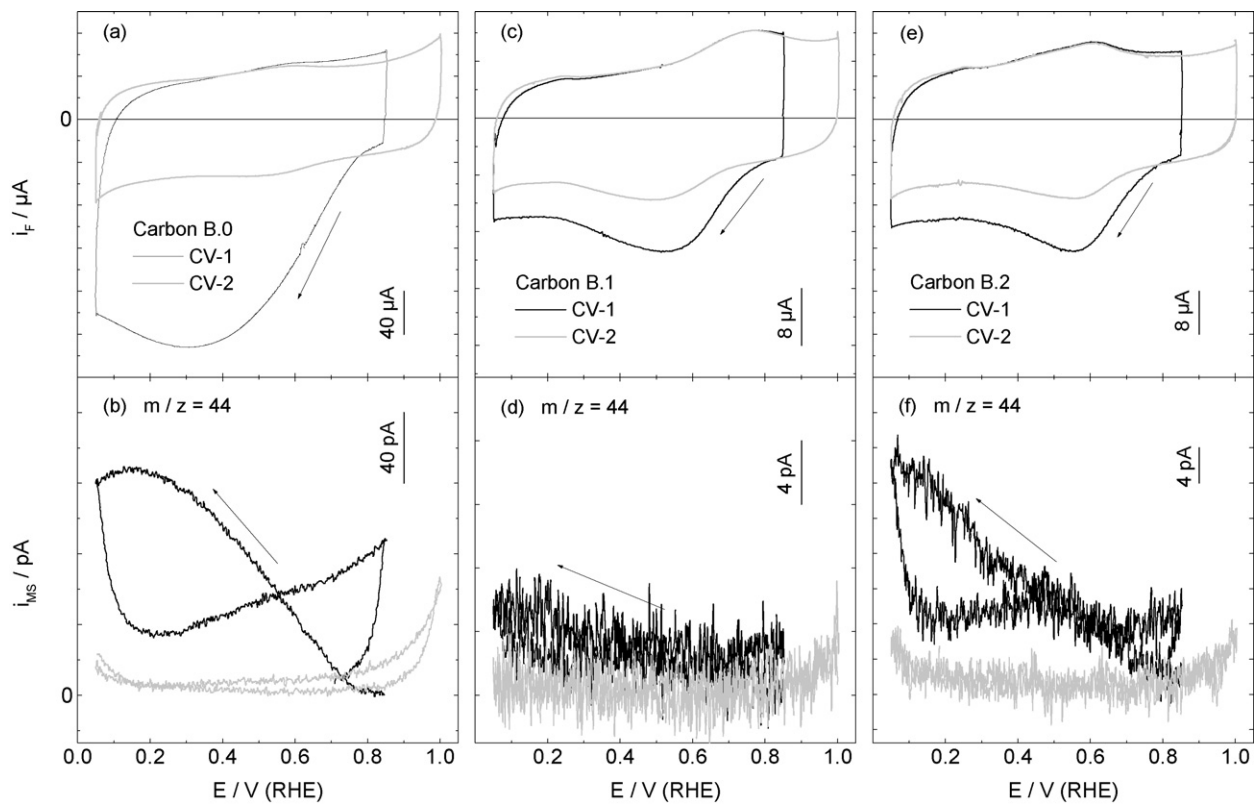


Fig. 5. Potential-dependent CO_2 generation: simultaneously recorded Faradaic (a, c and e) and mass spectrometric currents (b, d and f) on non-treated (B.0), graphitized (B.1) and graphitized/oxidized (B.2) carbon materials after a sequence of three potential excursions to $1.5V_{\text{RHE}}$ (holding time 60 s) and subsequent return to $0.85V_{\text{RHE}}$ (holding time 120 s) in Ar-saturated $0.5\text{ M H}_2\text{SO}_4$ at room temperature. CV-1 represents the initial CV after the potential excursion and CV-2 represents the stable CV after cycling the potential several times between 0.06 and $1.0V_{\text{RHE}}$ (scan rate 10 mV s^{-1} , electrolyte flow rate ca. $60\ \mu\text{l s}^{-1}$).

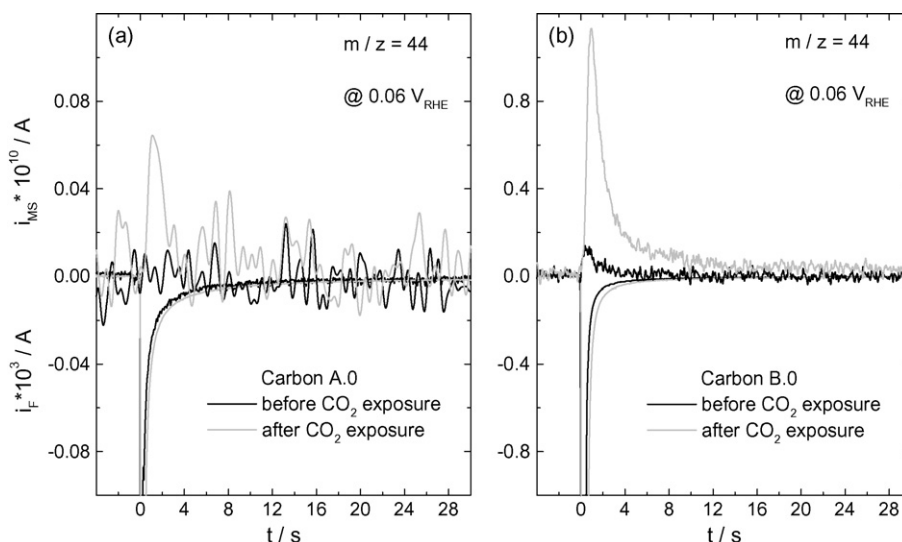


Fig. 6. Faradic (lower part) and mass spectrometric ($m/z = 44$; upper part) currents recorded at $0.06 V_{RHE}$ after exposing the carbon electrode (untreated materials: A.0 and B.0) to CO_2 -saturated and Ar-saturated $0.5 M H_2SO_4$ for 60 s at $1.0 V_{RHE}$. Following the CO_2 uptake, the potential was stepped from 1.0 to $0.06 V_{RHE}$ in Ar-saturated electrolyte (electrolyte flow rate ca. $60 \mu l s^{-1}$).

act weakly with carbonaceous surfaces, either via surface oxygen complexes or directly with graphene planes [60]. Accordingly, the release of CO_2 at low potentials could be induced by reduction of oxygenated surface carbon species, by potential induced destabilization of carbon–oxygen complexes or by charging/discharging of the carbon surface, which could be tentatively attributed to adsorption of bicarbonate anions, formed via hydration of CO_2 to carbonic acid, at higher potentials, and subsequent desorption of these anions at low potentials, resulting in (partial) dehydration of the released carbonic acid and CO_2 formation.

In all of these mechanisms for stabilizing CO_2 in the carbon pores or on the carbon surface, the amount of CO_2 stored in the carbon material would depend sensitively on the microstructure (porosity) of the carbon material. Stabilization of CO_2 in carbon nanopores fits well to the observation of the large amounts of CO_2 released at lower potentials from sample B.0, which exhibits the highest inner surface area (see Section 3.1). Decreasing the porosity results in less CO_2 release at low potentials. On the other hand, the very low amounts of CO_2 released on the graphitized samples A.1 and B.1, which have specific surface areas comparable to those of most other samples, but a very low surface oxygen contents, indicates that surface oxygen also plays an important role for the stabilization of CO_2 in the respective carbon materials.

To further examine the proposal of a potential induced release of adsorbed/trapped CO_2 , freshly prepared thin-film electrodes of the raw carbon materials (A.0 and B.0) were exposed to CO_2 -saturated supporting electrolyte at $1.0 V_{RHE}$ for 60 s, then the CO_2 -saturated electrolyte was fully exchanged by Ar-saturated electrolyte at the same potential, and finally the electrode potential was stepped back to $0.06 V_{RHE}$. Before, during and after the potential step, the CO_2 signal was followed by on-line mass spectrometry. For comparison, the same experiment was performed in Ar-saturated electrolyte (blank or reference experiment), without exposing the electrode to CO_2 (Fig. 6). Samples A.0 and B.0 were selected because of their significant difference in the total and internal surface area (porosity). Sample B.0 has an about 7.5 and 16 times higher total and internal surface area, respectively, compared to sample A.0.

Fig. 6a and b shows that for the blank experiments (black line), after exposing the electrodes at $1.0 V_{RHE}$ to Ar-saturated electrolyte and stepping the potential back to $0.06 V_{RHE}$, the sample A.0 does not produce any measurable amounts of CO_2 , whereas sample B.0 generated about $0.94 nC m^{-2}$ charge (normalized vs. the BET surface

area). The latter sample starts to be oxidized already at potential about $0.9 V_{RHE}$ (see Fig. 2b), therefore small amounts of CO_2 can be formed at $1.0 V_{RHE}$, which are partly released when stepping the potential back to $0.06 V_{RHE}$ in Ar-saturated electrolyte. The situation is quite different after exposing the samples to CO_2 -saturated electrolyte at $1.0 V_{RHE}$. After returning the potential to $0.06 V_{RHE}$, sample A.0 released an equivalent of about $3.5 nC m^{-2}$ of CO_2 , whereas sample B.0 produced an equivalent of ca. $13.3 nC m^{-2}$ or $9.2 \times 10^{15} CO_2$ molecules m^{-2} (light grey lines). For both samples, the Faradaic current transients do not show any significant change after exposure to Ar or CO_2 -saturated electrolyte at $1.0 V_{RHE}$. These results provide clear proof that measurable amounts of gaseous CO_2 can be stored in these carbon materials and released upon stepping to lower potentials. Considering that the uptake of CO_2 from the electrolyte may be diffusion limited, storage of CO_2 generated during the electrooxidation of carbon at high potentials in the carbon nanopores should be even more efficient. Furthermore, the simultaneous formation of oxygenated surface carbon species during electrooxidation of carbon at high potentials and their interaction with CO_2 will further enhance the amount of CO_2 stored in the respective carbon materials compared to the amounts observed in Fig. 6.

In total, these measurements clearly demonstrate that the CO_2 released from carbon supports at potentials well below the standard potential for carbon oxidation results at least partly from CO_2 which was formed during preceding excursions to high potentials and stabilized in the carbon material at these potentials. Additional contributions from CO_2 formation by chemical reaction between surface carbon and hydrogen peroxide formed at lower potentials via oxygen reduction can, however, not be excluded.

4. Conclusions

The oxidation and corrosion resistance of two different types of carbon supports for fuel cell catalysts, a little porous material (set A) and a highly porous material (set B), and the influence of subsequent graphitization or graphitization plus oxidation were investigated in model studies on thin-film electrodes under potential conditions relevant for PEFCs in mobile and stationary applications. Special attention was paid to the abnormal potential situation experienced during start-up and shut-down procedures, where the cathode potential can range up to $1.5 V_{RHE}$. Reversible surface oxidation to oxygenated surface carbon species and irreversible oxidation

to CO₂ could be discriminated by simultaneous electrochemical and mass spectrometric measurements. The specific surface area of the different materials was determined by adsorption measurements, discriminating between total surface area (nitrogen or iodine adsorption) and outer surface area (CTAB adsorption). The surface oxygen content was evaluated by XPS. These measurements led to the following results and conclusions:

1. For B-type carbon materials, the total specific surface area and the inner specific surface area or surface area of pores and voids of the non-treated material are significantly reduced by graphitization (high temperature treatment), they remain at that level upon subsequent thermal oxidation. For A-type carbon, the contributions from the pores (inner surface) are small, and subsequent treatments cause little changes in these characteristics. Even after processing, the (total) specific surface area of B-type carbon is about double of that of A-type carbon.
2. The absolute surface oxygen content determined by XPS analysis is significantly higher for B-type carbon than for A-type carbon, by 50–100%. For both materials, it decreases significantly upon graphitization, to about 40% of the original value, and increases sharply, to about 200–250% of the original value, upon subsequent thermal oxidation.
3. Reversible surface oxidation of carbon, which is evident by characteristic reduction/oxidation peaks at $\sim 0.5/\sim 0.6 V_{RHE}$, in base cyclic voltammograms, is largely correlated with the total surface area, in particular after excursion to high potentials ($1.5 V_{RHE}$).
4. The activity for irreversible oxidation of carbon to CO₂ at high potentials ($1.5 V_{RHE}$) decreases in the order graphitized/oxidized carbon > non-treated carbon > graphitized carbon, using the surface area normalized amount of CO₂ formed per time under these conditions as measure. This property depends little on the porosity, much more important is the amount or surface oxygen present before electrooxidation. Apparently, these surface species can act as nucleation sites or active centers for complete carbon oxidation. The observed decrease of CO₂ formation with increasing number of excursions to high potentials is tentatively explained by an increasing removal of active sites with specific structural (unsaturated carbon bonds) or chemical (oxygenated surface carbon species) properties during ongoing electrooxidation.
5. Based on CO₂ adsorption/desorption experiments, the apparent generation of CO₂ at low potentials below the standard potential for carbon ($0.207 V_{RHE}$ at 25 °C), e.g., in CVs recorded after electrochemical oxidation, can be explained by a potential induced release of CO₂ trapped in the pores and/or adsorbed on active carbon surface sites, where the CO₂ was formed during preceding exposure to high potentials. The amount of adsorbed/trapped CO₂ depends on the carbon micro- and nano-structure, with most CO₂ being observed on the highly porous non-treated B-type carbon. Depending on the nature of the adsorption/absorption process and the stabilizing interactions with the carbon surface, the adsorbed/trapped CO₂ can be released (i) by potential induced decomposition of stable surface carbon–oxygen complexes (decomposition to CO₂), (ii) by reduction of CO_{2,ad}-stabilizing oxygenated surface carbon species, or (iii) by physical charging of the interface.

Additional contributions from chemical reaction of surface carbon with hydrogen peroxide formed on the catalyst at low potentials in the presence of O₂ or air cannot be ruled out, but are not necessarily required to explain the observed CO₂ formation under these conditions.

In general, this model study on the corrosion stability of carbon showed that the graphitized materials with low oxygen surface content and low inner surface area (porosity) are most resis-

tant towards the reversible electrochemical carbon oxidation and towards irreversible oxidation of carbon under the abnormal PEFC operating conditions experienced during start-up/shut-down procedures.

Acknowledgements

This work was supported by the Federal Ministry of Education and Research within the network “KonnEkt” (BMBF, grant 03X2015D).

References

- [1] D. Thompsett, Fundamentals, Technology and Applications Fuel Cell Technology and Applications Part I, in: Handbook of Fuel Cells, vol. 3, Wiley & Sons, Chichester, 2003 (Chapter 37), p. 467;
- T. Tada, Fundamentals, Technology and Applications Fuel Cell Technology and Applications Part I, in: Handbook of Fuel Cells, vol. 3, Wiley & Sons, Chichester, 2003 (Chapter 37), p. 481;
- K. Ruth, M. Vogt, R. Zuber, Fundamentals, Technology and Applications Fuel Cell Technology and Applications Part I, in: Handbook of Fuel Cells, vol. 3, Wiley & Sons, Chichester, 2003 (Chapter 37), p. 489.
- [2] C. He, S. Desai, G. Brown, S. Bollepalli, *Interface* 2005 (2005) 41.
- [3] A.L. Dicks, *J. Power Sources* 156 (2006) 128.
- [4] G. Chen, S.R. Bare, T.E. Mallouk, *J. Electrochem. Soc.* 149 (2002) A1092–A1099.
- [5] R. Borup, J. Meyers, B. Pivovar, Y.S. Kim, R. Mukundan, N. Garland, D. Myers, M. Wilson, F. Garzon, D. Wood, P. Zelenay, K. More, K. Stroh, T. Zawodzinski, J. Boncella, J.E. McGrath, O.M. Inaba, K. Miyatake, M. Hori, K. Ota, Z. Ogumi, S. Miyata, A. Nihikata, Z. Siroma, Y. Uchimoto, K. Yasuda, K.-I. Kimijima, N. Iwashita, *Chem. Rev.* 107 (2007) 3904.
- [6] W. Schmittinger, A. Vahidi, *J. Power Sources* 180 (2008) 1.
- [7] J. Willsau, J. Heitbaum, *J. Electroanal. Chem.* 161 (1984) 93.
- [8] L.M. Roen, C.H. Paik, T.D. Jarvi, *Electrochem. Sol. Lett.* 7 (2004) 19.
- [9] J.P. Meyers, R.M. Darling, *J. Electrochem. Soc.* 153 (2006) A1432.
- [10] A.A. Franco, M. Gerard, *J. Electrochem. Soc.* 155 (2009) B367.
- [11] M.R. Tarasevich, V.A. Bogdanovskaya, N.M. Zagudaeva, *J. Electroanal. Chem.* 223 (1987) 161.
- [12] K. Kinoshita, *Carbon Electrochemical and Physicochemical Properties*, John Wiley & Sons, New York, 1988.
- [13] P.L. Antonucci, L. Pino, N. Giordano, G. Pinna, *Mater. Chem. Phys.* 21 (1989) 495.
- [14] N. Giordano, E. Passalacqua, L. Pino, A.S. Aricò, V. Antonucci, M. Vivaldi, K. Kinoshita, *Electrochim. Acta* 36 (1991) 1979.
- [15] K.H. Kangasniemi, D.A. Condit, T.D. Jarvi, *J. Electrochem. Soc.* 151 (2004) E125.
- [16] J. Li, C.W. Moore, D. Bhusari, S. Prakash, P.A. Kohl, *J. Electrochem. Soc.* 153 (2006) A343.
- [17] R.V. Hull, L. Li, Y. Xing, *Chem. Mater.* 18 (2006) 1780.
- [18] K.G. Gallagher, D.T. Wong, T.F. Fuller, *J. Electrochem. Soc.* 155 (2008) B488.
- [19] H.S. Oh, J.G. Oh, S. Haam, K. Arunabha, B. Roh, I. Hwang, H. Kim, *Electrochem. Commun.* 10 (2008) 1048.
- [20] F. Coloma, A. Septilveda-Escribano, J.L.G. Fierro, F. Rodríguez-Reinoso, *Langmuir* 10 (1994) 750.
- [21] P.J. Ferreira, G.J. la O', Y. Shao-Horn, D. Morgan, R. Makharia, S. Kocha, H.A. Gasteiger, *J. Electrochem. Soc.* 152 (2005) A2256.
- [22] K.J.J. Mayrhofer, S.J. Ashton, J.C. Meier, G.K.H. Wiberg, M. Hanzlik, M. Arenz, *J. Power Sources* 185 (2008) 734.
- [23] K.J.J. Mayrhofer, J.C. Meier, S.J. Ashton, G.K.H. Wiberg, F. Kraus, M. Hanzlik, M. Arenz, *Electrochem. Commun.* 10 (2008) 1144.
- [24] V.N. Antonov, J.H. Weaver, *Surf. Sci.* 526 (2003) 97.
- [25] M. Pourbaix, *Atlas of Electrochemical Equilibria in Aqueous Solution*, National Association of Corrosion Engineers, Houston, TX, 1979.
- [26] M. Inaba, H. Yamada, J. Tokunaga, A. Tasaka, *Electrochem. Solid State Lett.* 7 (2004) A474.
- [27] A. Schneider, L. Colmenares, Y.E. Seidel, Z. Jusys, B. Wickman, B. Kasemo, R.J. Behm, *Phys. Chem. Chem. Phys.* 10 (2008) 1931.
- [28] Y.E. Seidel, A. Schneider, Z. Jusys, B. Wickman, B. Kasemo, R.J. Behm, *Faraday Discuss.* 140 (2008) 167.
- [29] A. Bonakdarpour, C. Delacote, R. Yang, A. Wieckowski, R.J. Dahn, *Electrochem. Commun.* 10 (2008) 611.
- [30] M.F. Mathias, R. Makharia, H.A. Gasteiger, J.J. Conley, T.J. Fuller, C.J. Gittleman, S.S. Kocha, D.P. Miller, C.K. Mittelsteadt, T. Xie, S.G. Yan, P.T. Yu, *Interface* 14 (2005) 24.
- [31] C.A. Reiser, L. Bregoli, T.W. Patterson, J.S. Yi, J.D. Yang, M.L. Perry, T.D. Jarvi, *Electrochem. Solid-State Lett.* 8 (2005) A273.
- [32] Y. Tang, L. Zhang, Y. Wang, Y. Zhou, Y. Gao, C. Liu, W. Xing, T. Lu, *J. Power Sources* 162 (2006) 124.
- [33] W. Gu, R.N. Carter, P.T. Yu, H.A. Gasteiger, *ECS Trans.* 11 (2007) 963.
- [34] M.L. Perry, T.W. Patterson, C. Reiser, *ECS Trans.* 3 (2006) 783.
- [35] H. Yu, C. Ziegler, *J. Electrochem. Soc.* 153 (2006) A570.
- [36] S.C. Ball, S.L. Hudson, D. Thompsett, B. Theobald, *J. Power Sources* 171 (2007) 18.
- [37] N.R. Laine, F.J. Vastola, P.L. Walker Jr., *J. Phys. Chem.* 67 (1963) 2030.
- [38] M.T. Coltharp, N. Hackerman, *J. Phys. Chem.* 72 (1968) 1171.

- [39] H. Thiele, *Trans. Faraday Soc.* 34 (1938) 1033.
- [40] H. Binder, A. Kohling, K. Richter, G. Sandstede, *Electrochim. Acta* 9 (1964) 255.
- [41] M. Heinen, Y.X. Chen, Z. Jusys, R.J. Behm, *Electrochim. Acta* 52 (2007) 5634.
- [42] Z. Jusys, H. Massong, H. Baltruschat, *J. Electrochem. Soc.* 146 (1999) 1093.
- [43] Z. Jusys, J. Kaiser, R.J. Behm, *Phys. Chem. Chem. Phys.* 3 (2001) 4650.
- [44] T.J. Schmidt, H.A. Gasteiger, G.D. Stäb, P.M. Urban, D.M. Kolb, R.J. Behm, *J. Electrochem. Soc.* 145 (1998) 2354.
- [45] A. Schröder, M. Kluppel, R.H. Schuster, J. Heidberg, *Carbon* 40 (2002) 207.
- [46] A. Logadottir, T.H. Rod, J.K. Nørskov, B. Hammer, S. Dahl, C.J.H. Jacobsen, *J. Catal.* 197 (2001) 229.
- [47] C.H. Paik, G.S. Saloka, G.W. Graham, *Electrochem. Solid-State Lett.* 10 (2007) B39.
- [48] K. Kinoshita, J.A.S. Bett, *Carbon* 11 (1973) 403.
- [49] P. Stonehart, *Carbon* 22 (1984) 423.
- [50] M.R. Tarasevich, E.I. Khrushcheva, in: B.E. Conway, J.O. Bockris, R.E. White (Eds.), *Modern Aspects of Electrochemistry*, Plenum Press, New York, 1989, Chapter 5.
- [51] L. Li, Y. Xing, *J. Electrochem. Soc.* 153 (2006) A1823.
- [52] L. Li, Y. Xing, *J. Power Sources* 178 (2008) 75.
- [53] S. Maass, F. Finsterwalder, G. Frank, R. Hartmann, G. Merten, *J. Power Sources* 176 (2008) 444.
- [54] W.R. Baumgartner, P. Parz, S.D. Fraser, E. Wallnöfer, V. Hacker, *J. Power Sources* 182 (2008) 413.
- [55] K. Tammeveski, K. Kontturi, R.J. Nichols, R.J. Potter, D.J. Schiffrin, *J. Electroanal. Chem.* 515 (2001) 101.
- [56] F. Mirkhalaf, K. Tammeveski, D.J. Schiffrin, *Phys. Chem. Chem. Phys.* 6 (2004) 1321.
- [57] U.A. Paulus, T.J. Schmidt, H.A. Gasteiger, R.J. Behm, *J. Electroanal. Chem.* 495 (2001) 134.
- [58] Z. Jusys, J. Kaiser, R.J. Behm, *J. Electroanal. Chem.* 554–555 (2003) 427.
- [59] Z.Y. Liu, B.K. Brady, R.N. Carter, B. Litteer, M. Budinski, J.K. Hyun, D.A. Muller, *J. Electrochem. Soc.* 155 (2008) B979.
- [60] A. Montoya, F. Mondragón, T.N. Truong, *Carbon* 41 (2003) 29.
- [61] C. Ishizaki, I. Martí, *Carbon* 19 (1981) 409.